Comparison between homogeneous and separated flow models of isobutane flowing through adiabatic capillary tubes

Yonghui Shu, Peng Hu ✉, Ibrahim Adnan, Lianghui Zhi, and Qi Chen

Department of Thermal Science and Energy Engineering, University of Science and Technology of China, Hefei 230027, China

✉Correspondence: Peng Hu, E-mail: hupeng@ustc.edu.cn

Graphical abstract

Simulation on the throttling process of refrigerant flowing through adiabatic capillary tubes.

Public summary

■ Homogeneous flow models and separated flow models with and without metastable flow are compared in detail.

■ The optimal hypothesis models for different R600a mass flow rate ranges are investigated.

■ The optimal combinations of friction factor and two-phase viscosity correlations for each model are recommended.

Comparison between homogeneous and separated flow models of isobutane flowing through adiabatic capillary tubes
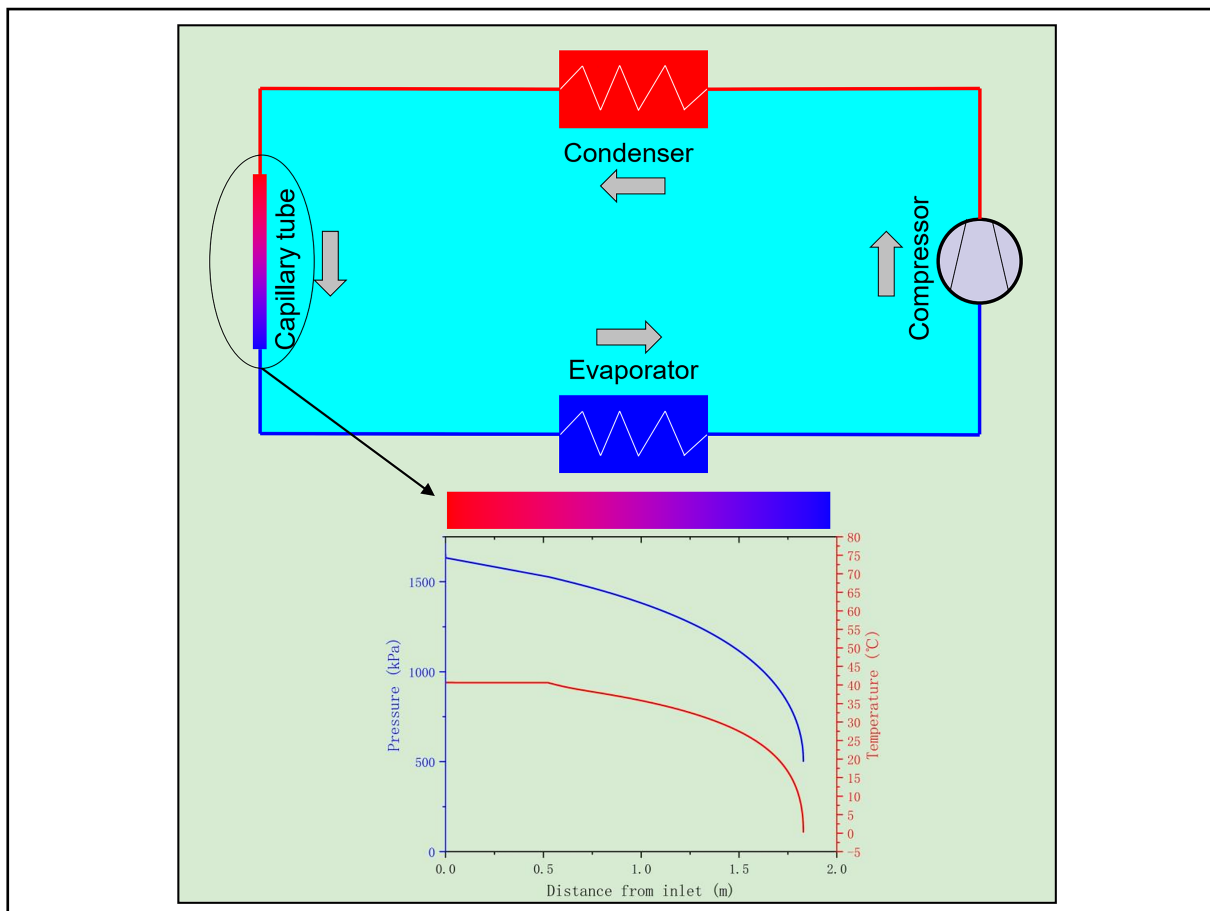
Yonghui Shu, Peng Hu ✉, Ibrahim Adnan, Lianghui Zhi, and Qi Chen

Department of Thermal Science and Energy Engineering, University of Science and Technology of China, Hefei 230027, China

✉Correspondence: Peng Hu, E-mail: hupeng@ustc.edu.cn

Cite This: *JUSTC*, **2022**, 52(7): 5 (14pp)   Read Online

Abstract: Capillary tubes have been widely used as expansion devices in small-scale refrigeration and heat-pump systems. However, adiabatic flow through a capillary tube is extremely complicated, despite its simple geometry. This work presents a comparative study on the homogenous flow model and separated flow model, which were used to simulate the flow of isobutene (R600a) through adiabatic capillary tubes. The influence of different combinations of friction factor and two-phase viscosity correlations, and the effect of metastable flow on the flow characteristics were investigated. The predicted mass flow rate was lower when the separated flow model was used. The separated flow model performed better in predicting a mass flow rate over 2 kg·h⁻¹. The Colebrook friction factor correlation combined with the Dukler or McAdams viscosity correlation yielded smaller deviations of 5.43%, 5.49% and 5.44%, 5.43% when ignoring and considering the metastable flow, respectively. Additionally, the homogenous flow model adopting the Bittle and Pate friction factor and Dukler viscosity correlations achieved the highest accuracy with a mass flow rate under 2 kg·h⁻¹. The mean error was 4.12% in the case without metastable flow, and 3.37% in the case with metastable flow.

Keywords: capillary tube; adiabatic flow; friction factor; two-phase viscosity; homogeneous flow model; separated flow model; metastable flow

CLC number: O551.3   **Document code:** A

Nomenclature		Subscripts	
A	cross-sectional area (m²)	c	critical
d	differential sign	cond	condenser
dL	control volume length (m)	egl	equilibrium two-phase
D	inner diameter (m)	eva	evaporator
f	friction factor	g	vapor phase
G	mass flux (kg·m⁻²·s⁻¹)	$i,i+1...$	interface number of the control volume
h	specific enthalpy (J·kg⁻¹)	in	inlet
k	Boltzmann constant	l	liquid phase
K	entrance loss coefficient	m	average
L	length (m)	mgl	metastable two-phase
m	mass flow rate (kg·s⁻¹)	ml	metastable liquid phase
P	pressure (Pa)	out	outlet
Re	Reynolds number	sat	saturated
S	slip ratio	sc	subcooled
T	temperature (℃)	sg	saturated vapor phase
U	wetted perimeter (m)	sl	saturated liquid phase
v	specific volume (m³·kg⁻¹)	total	total
V	velocity (m·s⁻¹)	vap	vaporization
x	mass fraction	w	wall
y	mass fraction of saturated phase		

Greek letters		Abbreviations	
α	void fraction	ODP	ozone depletion potential
ρ	density (kg·m⁻³)	GWP	global warming potential
τ	shear stress (N·m⁻²)	CFCs	chlorofluorocarbons
σ	surface tension (N·m⁻¹)	HCFCs	hydrochlorofluorocarbons
ε	tube wall roughness (m)	HCs	hydrocarbons
μ	dynamic viscosity (Pa·s)		

1 Introduction

To mitigate environmental issues, the refrigeration industry has gradually discarded the usage of CFC and HCFC refrigerants owing to their higher ODP and GWP. Nowadays, researchers worldwide are focusing on environmentally benign refrigerants[1]. The thermophysical properties[2−5] of these environmentally-sound fluids and their uses[6−9] have been comprehensively investigated. Hydrocarbon refrigerants, such as isobutene (R600a), have great potential as alternatives to conventional refrigerants. These refrigerants have beneficial performance owing to their lower critical pressure, higher enthalpy difference between the two-phase regions, zero ODP, and lower GWP.

Capillary tubes are commonly used to expand and control the flow of refrigerants in small cooling and heating systems, including domestic refrigerators[10], miniaturized cooling

systems[11], cryogenic systems[12−14], and heat pump systems[15]. Typically, the geometry of a capillary tube is somewhat simple with a diameter ranging from 0.5 mm to 2.0 mm and length ranging from 2 m to 6 m[16]. The capillary tube has wider applications owing to its simplicity, reliability, and low cost. However, the flow through the capillary tube is very complicated owing to the simultaneous pressure drop and phase change of the refrigerant[17]. Because of the drastic change in the refrigerant properties in a two-phase flow through a capillary tube, it is impossible to describe the entire throttling process analytically and explicitly[18].

Many previous studies have adopted finite-volume-based methods[19, 20], empirical correlations[21], and algebraic equations[22] to predict the thermal and fluid-dynamic characteristics, and investigated suitable sizes for designing the capillary tube. Among the three above-mentioned approaches, the finite-volume-based method is the only method that can simulate the pressure and temperature distributions along a capillary tube, and can also predict the mass flow rate or tube length, which is the main objective of empirical correlations and algebraic equations with given boundary conditions.

In recent decades, several numerical models based on finite-volume methods have been established and modified by researchers to rapidly simulate the flow process. Khan et al.[16], Dubba and Kumar[23] extensively reviewed previous numerical investigations. Homogeneous and separated flow models have been widely used in the two-phase region in the simulation of flow through a capillary tube. Jadhav and Agrawal[24] numerically investigated the flow characteristics of straight and spiral adiabatic capillary tubes using a homogeneous-flow model. Compared with straight tubes, a reduction of 22% and 15% in the mass flow rate was observed in spiral tubes with CO_2 and R22 refrigerants, respectively. Alok and Sahu[25] employed a homogeneous model for computation using ANSYS CFX with user-defined properties. The mean deviations in the mass flow rates of R12, R22, R134a, R410A, and R32 in the straight capillary tube were compared to experimental data reported in the literature. Recently, Jadhav and Agrawal[26] conducted a numerical investigation using a homogeneous model, and compared the flow behavior of adiabatic spiral and helical capillary tubes in a CO_2 transcritical system. The reduction in the mass flow rate of the spiral capillary tubes was higher by 18% compared with that of helical capillary tubes. Zareh et al.[27] used a separated model to simulate the flow of R12, R22, and R134a refrigerants through straight and helically adiabatic capillary tubes, and found that the mass flux, coiled diameter, and tube diameter increased linearly with the degree of subcooling. However, the above-mentioned models did not consider the metastable flow phenomenon. Wang et al.[28] developed a separated flow model considering metastable flow to investigate the flow in the coiled adiabatic capillary tubes of a CO_2 transcritical system. Their results revealed that the metastable flow region has negligible influence on the calculated capillary length, owing to the large under-pressure caused by high inlet pressure.

The homogeneous flow model assumes that the liquid and vapor phases have the same velocity, and that the fluid properties of the mixture can be considered as the mean properties of the liquid and vapor phases. In contrast, the separated flow model considers the velocity slip and property differences between the liquid and vapor phases. Despite the universal utilization of the two models, few comparative studies have been conducted. Agrawal and Bhattacharyya[29] used the homogeneous flow and separated flow models and compared the flow characteristics of adiabatic capillary tubes in a transcritical CO_2 heat pump system. Their results revealed that the maximum discrepancy between the two models was approximately 8%–11%. However, the models were validated by considering experimental data for R22 only, because CO_2 data were not available. Another comparative study using three different refrigerants was conducted by Furlong and Schmidt[30]. In their study, the separated flow model outperformed the homogeneous flow model in all cases. The mean error of the separated flow model was 5.77%, 4.57%, and 8.03% for R134a, R600a, and R744, respectively. However, the study mentioned above considered neither the effects of metastable flow nor different combinations of friction factor and two-phase viscosity correlations.

Lorbek et al.[31] experimentally investigated the flow visualization of R600a flowing through a straight capillary tube made of fluorinated ethylene propylene polymer. An increase in the average velocity of the vapor phase was observed as the mass flow rate increased, and the difference between the velocity of the vapor and liquid phase had the same tendency. Additionally, different surface textures had different effects on the flow pattern and flow homogeneity. Therefore, it is important that an appropriate flow pattern assumption and numerical model are used in the simulation of flow through capillary tubes. However, simulation studies considering the effect of the mass flow rate on the accuracy of different models have not been conducted to date.

To investigate the optimal mass flow rate ranges for both the homogenous flow model and separated flow model, this study used two models to conduct a comparative investigation on R600a flowing through adiabatic capillary tubes with and without a metastable flow region. Compared with previous simulation studies, this study used more comprehensive models and easier calculation methods. The predicted mass flow rates were compared to the experimental data obtained by Melo et al.[32] and Schenk and Oellrich[18] to assess the model accuracy. Finally, this study assessed the effects of various friction factor correlations and two-phase viscosity correlations.

2 Model descriptions

Fig. 1 shows the schematic diagram of an adiabatic capillary tube in the cases with and without metastable flow. In the case of metastable flow, all four regions are considered; in the case without metastable flow, the metastable liquid region and metastable two-phase region are ignored.

In both cases, the capillary tube is divided into small control volumes in terms of length, as shown in Fig. 2. The differential governing equations are solved discretely for every small control volume. To simplify the establishment of the numerical models, the following assumptions are made.

(A1) The capillary tube is straight and horizontally placed; therefore, the gravitational potential energy can be ignored.

(A2) The inner diameter and roughness are constant along the entire capillary tube.

(A3) The flow through the capillary tube is one-dimensional, adiabatic, steady, and has no input or output.

(A4) The refrigerant is free of impurities.

These assumptions may result in certain deviations between the simulation and the actual situation; therefore, the model accuracy is a fundamental point to be investigated.

2.1 Entrance sudden contraction

As shown in Fig. 1, owing to the sudden contraction between the condenser and the inlet of the capillary tube, a local pressure loss must exist. The pressure loss at the entrance, which is caused by sudden contraction, can be calculated as follows[33]:

$$P_{cond} - P_{in} = (1 + K) \frac{\rho V^2}{2}, \qquad (1)$$

where K is the entrance loss coefficient, which is equal to 0.5 for a sharp edge entrance.

2.2 Subcooled liquid region

After the subcooled liquid refrigerant enters the capillary tube, the pressure along the tube decreases under the action of friction. The subcooled-liquid region is defined as the region from the entrance to the point where the saturated pressure corresponds to the inlet temperature ($P_{sat,in}$). The mass, momentum, and energy conservation equations for the subcooled-liquid region are expressed as follows:

Mass conservation equation:

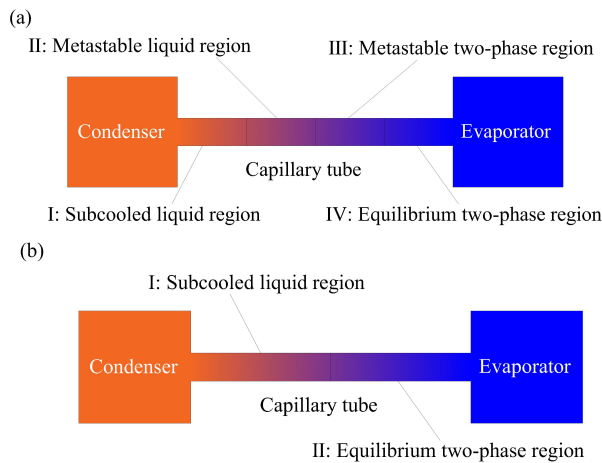$$\mathrm{d}m = \mathrm{d}(GA) = \mathrm{d}(\rho VA) = 0. \qquad (2)$$

(a)

(b)

Fig. 1. Schematic diagram of adiabatic capillary tube. (a) Case with metastable flow. (b) Case without metastable flow.
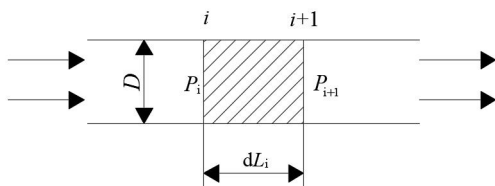
Fig. 2. Control volume of adiabatic capillary tube.

Momentum conservation equation:

$$A \frac{\mathrm{d}P}{\mathrm{d}L} + \frac{\mathrm{d}(\rho A V^2)}{\mathrm{d}L} + \tau_w U = 0, \qquad (3)$$

where the wall shear stress is modeled as follows:

$$\tau_w = \frac{f \rho V^2}{8}. \qquad (4)$$

Energy conservation equation:

$$\mathrm{d}\left[m\left(h + \frac{V^2}{2}\right)\right] = 0. \qquad (5)$$

Many previous studies[27−29] have assumed that the sub-cooled liquid refrigerant is incompressible with constant specific volume and specific enthalpy over the entire region. Hence, the length of the subcooled-liquid region can be directly calculated using the momentum conservation equation. To improve the calculation accuracy, this assumption was not adopted in this study.

For every small control volume shown in Fig. 2, the differential governing equations can be dispersed and solved. When the control-volume pressure drop is known, the length of every control volume in the subcooled liquid region can be determined as follows:

$$\Delta L_{sc} = \frac{2D}{G^2 f_{sc,m} v_{sc,m}} \left[\Delta P - G^2 (v_{i+1} - v_i)\right]. \qquad (6)$$

Therefore, the length of the entire region (L_{sc}) can be obtained by accumulating all control volume lengths. The correlations used to calculate the friction factors are discussed in the next section.

2.3 Metastable liquid region

When the pressure drop along the capillary tube decreases to $P_{sat,\ in}$, the refrigerant begins to evaporate. Actually, the initial point of evaporation (P_{vap}) is somewhere after $P_{sat,\ in}$, which means that the evaporation is delayed owing to the surface tension of the refrigerant. The region from $P_{sat,\ in}$ to P_{vap} is defined as the metastable liquid region wherein the liquid refrigerant is superheated. The difference in the value ($P_{sat,\ in} - P_{vap}$) between the two above-mentioned pressures is called the under-pressure.

To the best of the authors' knowledge, a precise method for calculating the under-pressure has not been proposed. The most commonly used formula for calculating the under-pressure has been proposed by Chen et al.[34], and is based on nucleation theory; the formula is:

$$\frac{(P_{sat,in} - P_{vap})\ \sqrt{kT_{sat}}}{\sigma^{\frac{3}{2}}} = 0.679 \left(\frac{v_g}{v_g - v_l}\right) Re^{0.941} \left(\frac{\Delta T_{sc}}{T_c}\right)^{-0.208} \left(\frac{D}{D'}\right)^{-3.18}, \qquad (7)$$

where ΔT_{sc} is the degree of subcooling, and D' is the reference length defined as:

$$D' = \sqrt{\frac{kT_{sat}}{\sigma}} \times 10^4. \qquad (8)$$

The refrigerant properties in this region correspond to the outlet liquid temperature of the subcooled-liquid region. The governing equations of the metastable liquid region are the

same as those of the subcooled-liquid region. Therefore, the total length of the metastable liquid region can be obtained using Eq. (3), as follows:

$$L_{\mathrm{ml}} = \frac{2D(P_{\mathrm{sat,in}} - P_{\mathrm{vap}})}{G^2 f_{\mathrm{ml}} v_{\mathrm{ml}}}. \tag{9}$$

2.4 Metastable two-phase region

The metastable two-phase region begins at the point where the first bubble appears; that is, at the point where the refrigerant reaches thermodynamic equilibrium. Feburie et al.[35] considered this region as a three-phase region, including superheated liquid, saturated liquid, and saturated vapor. The mass fraction of the vapor phase (x_{g}) and mass fraction of the saturated phase (y) is introduced to describe the components of this region:

$$x_{\mathrm{g}} = \frac{m_{\mathrm{sg}}}{m_{\mathrm{ml}} + m_{\mathrm{sl}} + m_{\mathrm{sg}}}, \tag{10}$$

$$y = \frac{m_{\mathrm{sl}} + m_{\mathrm{sg}}}{m_{\mathrm{ml}} + m_{\mathrm{sl}} + m_{\mathrm{sg}}}. \tag{11}$$

The bubbles are surrounded by a saturated liquid, whereas some superheated liquid is dispersed between the bubbles. Heat transfer and mass transfer occur simultaneously between the superheated and saturated phases owing to temperature differences. The mass fraction of the saturated phase can be determined using the following mass-transfer equation[35]:

$$\frac{\mathrm{d}y}{\mathrm{d}L} = 0.02\left(\frac{U}{A}\right)(1-y)\left(\frac{P_{\mathrm{sat}} - P}{P_{\mathrm{c}} - P_{\mathrm{sat}}}\right)^{0.25}. \tag{12}$$

2.4.1 Homogenous flow model

For the homogenous flow model, the governing equations of the two-phase region are the same as those of the liquid region, owing to the uniformity of the velocities of the liquid and vapor phases. Therefore, variable L can be eliminated by combining Eqs. (3) and (12) to simplify the solution of the equation. The equation dispersed in the control volume is:

$$\frac{f_{\mathrm{mgl,m}} G^2 v_{\mathrm{mgl,m}} [\ln(1-y_{i+1}) - \ln(1-y_i)]}{0.16} = $$
$$[P_{i+1} - P_i + G^2(v_{i+1} - v_i)]\left(\frac{P_{\mathrm{sat}} - P_{\mathrm{m}}}{P_{\mathrm{c}} - P_{\mathrm{sat}}}\right)^{0.25}. \tag{13}$$

The average specific volume and specific enthalpy of the metastable two-phase refrigerant can be calculated using the weighted average value of the three phases, as follows:

$$h_{\mathrm{mgl}} = (1-y)h_{\mathrm{ml}} + (y-x_{\mathrm{g}})h_{\mathrm{sl}} + x_{\mathrm{g}}h_{\mathrm{sg}}, \tag{14}$$

$$v_{\mathrm{mgl}} = (1-y)v_{\mathrm{ml}} + (y-x_{\mathrm{g}})v_{\mathrm{sl}} + x_{\mathrm{g}}v_{\mathrm{sg}}. \tag{15}$$

In this region, the properties of the superheated liquid are the same as those in the metastable liquid region, and the

properties of the saturated liquid and vapor correspond to the local pressure. The two above-mentioned equations can be substituted into the dispersed energy conservation equation:

$$h_i + \frac{G^2 v_i^2}{2} = h_{\mathrm{ml}} + y_{i+1}(h_{\mathrm{sl},i+1} - h_{\mathrm{ml}}) + x_{\mathrm{g},i+1}(h_{\mathrm{sg},i+1} - h_{\mathrm{sl},i+1}) +$$
$$\frac{G^2[v_{\mathrm{ml}} + y_{i+1}(v_{\mathrm{sl},i+1} - v_{\mathrm{ml}}) + x_{\mathrm{g},i+1}(v_{\mathrm{sg},i+1} - v_{\mathrm{sl},i+1})]^2}{2}. \tag{16}$$

Eqs. (13) and (16) have the common unknown variables $x_{\mathrm{g},i+1}$ and y_{i+1} in every control volume of the metastable two-phase region. Therefore, all parameters can be obtained by iteratively solving the two equations. The average temperature of this region can be calculated using the weighted average temperature of the superheated and saturated phases:

$$T_{\mathrm{mgl}} = (1-y)T_{\mathrm{ml}} + yT_{\mathrm{sat}}. \tag{17}$$

The total length of the metastable two-phase region (L_{mgl}) can be calculated using the method used for the subcooled-liquid region.

2.4.2 Separated flow model

In the separated flow model, the flow is segregated into two streams: liquid and vapor. The separated flow model is the most valid model for annular flow patterns, owing to its consideration of various flow patterns[29]. The mass, momentum, and energy conservation equations in the two-phase region are:
Mass conservation equation:

$$\mathrm{d}m = \mathrm{d}(\rho_{\mathrm{l}} V_{\mathrm{l}} A_{\mathrm{l}}) + \mathrm{d}(\rho_{\mathrm{g}} V_{\mathrm{g}} A_{\mathrm{g}}) = 0. \tag{18}$$

Momentum conservation equation:

$$(A_{\mathrm{l}} + A_{\mathrm{g}})\frac{\mathrm{d}P}{\mathrm{d}L} + \frac{\mathrm{d}\left(\rho_{\mathrm{l}} A_{\mathrm{l}} V_{\mathrm{l}}^2 + \rho_{\mathrm{g}} A_{\mathrm{g}} V_{\mathrm{g}}^2\right)}{\mathrm{d}L} + \tau_{\mathrm{w}} U = 0. \tag{19}$$

For the annular flow pattern, the wall shear stress is defined as follows:

$$\tau_{\mathrm{w}} = \frac{f \rho_{\mathrm{l}} V_{\mathrm{l}}^2}{8}. \tag{20}$$

Energy conservation equation:

$$\mathrm{d}\left[m_{\mathrm{l}}\left(h_{\mathrm{l}} + \frac{V_{\mathrm{l}}^2}{2}\right) + m_{\mathrm{g}}\left(h_{\mathrm{g}} + \frac{V_{\mathrm{g}}^2}{2}\right)\right] = 0. \tag{21}$$

The mass flow rate and velocity of the two phases are functions of the vapor-phase mass fraction and void fraction, respectively:

$$m_{\mathrm{l}} = GA(1-x_{\mathrm{g}}), \tag{22}$$

$$m_{\mathrm{g}} = GAx_{\mathrm{g}}, \tag{23}$$

$$V_{\mathrm{l}} = \frac{G(1-x_{\mathrm{g}})v_{\mathrm{g}}}{1-\alpha}, \tag{24}$$

$$V_{\mathrm{g}} = \frac{Gx_{\mathrm{g}}v_{\mathrm{g}}}{\alpha}. \tag{25}$$

The void fraction calculation adopts the Premoli correlaion[28, 29, 36]:

$$\alpha = \frac{x_{\mathrm{g}} \nu_{\mathrm{g}}}{(1 - x_{\mathrm{g}}) \nu_{\mathrm{l}} S + x_{\mathrm{g}} \nu_{\mathrm{g}}}, \tag{26}$$

where the slip ratio between the two phases is given by the Chisholm correlation[28, 29, 37]

$$S = \left[1 - x_{\mathrm{g}} \left(1 - \frac{\rho_{\mathrm{l}}}{\rho_{\mathrm{g}}} \right) \right]^{0.5}. \tag{27}$$

In the metastable two-phase region, the superheated liquid is assumed to have no slip against the saturated liquid. Therefore, the specific volume and specific enthalpy values of the liquid phase in this region are the average values of the superheated and saturated liquids. The following discrete equation can be obtained after rearranging and dispersing Eqs. (12) and (19):

$$\frac{f_{\mathrm{mgl,m}} G^2 (1 - x_{\mathrm{g,m}})^2 \nu_{\mathrm{l,m}} \left[\ln(1 - y_{i+1}) - \ln(1 - y_i) \right]}{0.16} = \left(\frac{P_{\mathrm{sat}} - P_{\mathrm{m}}}{P_{\mathrm{c}} - P_{\mathrm{sat}}} \right)^{0.25} \times$$
$$\left[P_{i+1} - P_i + G^2 \left(\frac{(1 - x_{\mathrm{g},i+1})^2 \nu_{\mathrm{l},i+1}}{1 - \alpha_{i+1}} + \frac{x_{\mathrm{g},i+1}{}^2 \nu_{\mathrm{sg},i+1}}{\alpha_{i+1}} - \frac{(1 - x_{\mathrm{g},i})^2 \nu_{\mathrm{l},i}}{1 - \alpha_i} - \frac{x_{\mathrm{g},i}{}^2 \nu_{\mathrm{sg},i}}{\alpha_i} \right) \right]. \tag{28}$$

The discrete form of the energy conservation equation in the metastable two-phase region is expressed as follows:

$$x_{\mathrm{g},i} h_{\mathrm{sg},i} + (y_i - x_i) h_{\mathrm{sl},i} + (1 - y_i) h_{\mathrm{ml},i} + x_{\mathrm{g},i} \frac{V_{\mathrm{sg},i}^2}{2} + (1 - x_{\mathrm{g},i}) \frac{V_{\mathrm{l},i}^2}{2} =$$
$$x_{\mathrm{g},i+1} h_{\mathrm{sg},i+1} + (y_{i+1} - x_{i+1}) h_{\mathrm{sl},i+1} + (1 - y_{i+1}) h_{\mathrm{ml},i+1} + x_{\mathrm{g},i+1} \frac{V_{\mathrm{sg},i+1}^2}{2} + (1 - x_{\mathrm{g},i+1}) \frac{V_{\mathrm{l},i+1}^2}{2}. \tag{29}$$

For the convenience of programming, variables $x_{\mathrm{g},i+1}$ and y_{i+1} can be obtained iteratively by combining Eqs. (28) and (29) instead of using the matrix solution. The average temperature and total length of this region are calculated using the same method as that used for the homogenous flow model.

2.5 Equilibrium two-phase region

When the entire superheated liquid enters the saturated state, which means that the mass fraction of the saturated phase (y) equals unity, the refrigerant flow reaches equilibrium. To describe the refrigerant state in this region, only the mass fraction of the vapor phase (x_{g}) is required. The temperature of this region equals the saturated temperature corresponding to the local pressure.

For the homogenous flow model, the average specific volume and specific enthalpy are expressed without metastable liquid items, as follows:

$$h_{\mathrm{egl}} = (1 - x_{\mathrm{g}}) h_{\mathrm{l}} + x_{\mathrm{g}} h_{\mathrm{g}}, \tag{30}$$

$$\nu_{\mathrm{egl}} = (1 - x_{\mathrm{g}}) \nu_{\mathrm{l}} + x_{\mathrm{g}} \nu_{\mathrm{g}}. \tag{31}$$

Hence, the discrete energy conservation equation is:

$$h_i + \frac{G^2 \nu_i^2}{2} = h_{\mathrm{l},i+1} + x_{\mathrm{g},i+1} (h_{\mathrm{g},i+1} - h_{\mathrm{l},i+1}) + \frac{G^2 [\nu_{\mathrm{l},i+1} + x_{\mathrm{g},i+1} (\nu_{\mathrm{g},i+1} - \nu_{\mathrm{l},i+1})]^2}{2}. \tag{32}$$

For the separated flow model, the equation becomes:

$$x_{\mathrm{g},i} h_{\mathrm{sg},i} + (1 - x_i) h_{\mathrm{sl},i} + x_{\mathrm{g},i} \frac{V_{\mathrm{sg},i}^2}{2} + (1 - x_{\mathrm{g},i}) \frac{V_{\mathrm{sl},i}^2}{2} =$$
$$x_{\mathrm{g},i+1} h_{\mathrm{sg},i+1} + (1 - x_{i+1}) h_{\mathrm{sl},i+1} + x_{\mathrm{g},i+1} \frac{V_{\mathrm{sg},i+1}^2}{2} + (1 - x_{\mathrm{g},i+1}) \frac{V_{\mathrm{sl},i+1}^2}{2}. \tag{33}$$

Variable $x_{\mathrm{g},i+1}$ can be obtained based on Eq. (33), and all other parameters can be obtained accordingly. Similarly, the total length of the equilibrium two-phase region (L_{egl}) can be calculated using the momentum-conservation equation.

2.6 Choked flow conditions

Choked flow generally exists at the exit of capillary tubes[38]. The choking phenomenon of the refrigerant in the capillary tubes is similar to the isentropic flow of gas passing through a converging nozzle. When the refrigerant reaches the choked flow condition, the Mach number equals unity and the entropy of the refrigerant reaches its maximum value. Most importantly, once the flow reaches the choking condition, the downstream pressure does not influence the mass flow rate. Therefore, the maximum mass flow rate occurs in every capillary tube with a fixed tube length.

Several criteria for detecting choked flow conditions, such as entropy, Mach number, and length criteria, have been proposed. Among them, the length criterion derived by Chung[39] from the entropy criterion is the easiest to apply in the proposed numerical models because the only required physical parameter is the control volume length. The flow reaches the choked condition when the calculation result of the control volume length in the equilibrium two-phase region reaches zero or a negative value. In the present study, this criterion was selected because of its simplicity and high accuracy.

3 Friction factor and two-phase viscosity correlations

3.1 Friction factor correlations

For homogenous or separated flow models, the friction factor is a key factor for accurately predicting the characteristics of refrigerants flowing through capillary tubes. Three different friction factor correlations were assessed and compared using the proposed model. The three friction factor correlations[40] are:

Colebrook correlation:

$$\frac{1}{\sqrt{f}} = 1.14 - 2 \ln \left[\frac{\varepsilon}{D} + \frac{9.3}{Re \sqrt{f}} \right]; \tag{34}$$

Churchill correlation:

$$f = 8 \left[\left(\frac{8}{Re} \right)^{12} + \frac{1}{(A + B)^{\frac{3}{2}}} \right]^{\frac{1}{12}}, \tag{35}$$

where

$$A = \left\{ 2.457 \ln \left[\frac{1}{\left(\frac{7}{Re} \right)^{0.9} + \frac{0.27 \varepsilon}{D}} \right] \right\}^{16}, \tag{36}$$

$$B = \left(\frac{37530}{Re}\right)^{16}; \qquad (37)$$

Bittle and Pate correlation:

$$f = 0.23Re^{-0.216}. \qquad (38)$$

Both the Reynolds number and tube wall roughness are important parameters for calculating the friction factor. However, the Bittle and Pate correlations only consider the influence of the Reynolds number.

3.2 Two-phase viscosity correlations

Dynamic viscosity is a crucial property owing to its effect on fluid motion and friction[41]. In both models, the viscosity of the liquid phase is used to calculate the Reynolds numbers in the subcooled liquid and metastable liquid regions, whereas the average viscosity of the liquid and vapor phases is used in the metastable two-phase region and equilibrium two-phase region. Therefore, an appropriate viscosity correlation is important for accurately simulating capillary tube flow.

There are four classical two-phase viscosity correlations[40]. The Cicchitti correlation deviates from reality, therefore, the three following correlations were adopted:
McAdams correlation:

$$\frac{1}{\mu_{\mathrm{egl}}} = \frac{(1-x_{\mathrm{g}})}{\mu_{\mathrm{l}}} + \frac{x_{\mathrm{g}}}{\mu_{\mathrm{g}}}; \qquad (39)$$

Dukler correlation:

$$\mu_{\mathrm{egl}} = \frac{(1-x_{\mathrm{g}})\,v_{\mathrm{l}}\mu_{\mathrm{l}} + x_{\mathrm{g}}v_{\mathrm{g}}\mu_{\mathrm{g}}}{(1-x_{\mathrm{g}})\,v_{\mathrm{l}} + x_{\mathrm{g}}v_{\mathrm{g}}}; \qquad (40)$$

Lin correlation:

$$\mu_{\mathrm{egl}} = \frac{\mu_{\mathrm{l}}\mu_{\mathrm{g}}}{\mu_{\mathrm{g}} + x_{\mathrm{g}}^{1.4}(\mu_{\mathrm{l}} - \mu_{\mathrm{g}})}. \qquad (41)$$

For the equilibrium two-phase region, the three above-mentioned correlations can be used directly to calculate the average two-phase viscosity. Nevertheless, the average viscosity of the metastable two-phase region must include the viscosity of the superheated liquid. Contrary to previously established models[40,42], this study introduced three-phase mixed methods for the first two correlations. For the Lin correlation, the mixed viscosity of the superheated liquid and saturated liquid was determined before the results were input into Eq. (44) to calculate the metastable two-phase viscosity. The average viscosity correlations for the metastable two-phase region are:
McAdams correlation:

$$\frac{1}{\mu_{\mathrm{mgl}}} = \frac{(1-y)}{\mu_{\mathrm{ml}}} + \frac{(y-x_{\mathrm{g}})}{\mu_{\mathrm{sl}}} + \frac{x_{\mathrm{g}}}{\mu_{\mathrm{sg}}}; \qquad (42)$$

Dukler correlation:

$$\mu_{\mathrm{mgl}} = \frac{(1-y)\,v_{\mathrm{ml}}\mu_{\mathrm{ml}} + (y-x_{\mathrm{g}})\,v_{\mathrm{sl}}\mu_{\mathrm{sl}} + x_{\mathrm{g}}v_{\mathrm{sg}}\mu_{\mathrm{sg}}}{(1-y)\,v_{\mathrm{ml}} + (y-x_{\mathrm{g}})\,v_{\mathrm{sl}} + x_{\mathrm{g}}v_{\mathrm{sg}}}; \qquad (43)$$

Lin correlation:

$$\mu_{\mathrm{mgl}} = \frac{\mu_{\mathrm{l}}\mu_{\mathrm{sg}}}{\mu_{\mathrm{sg}} + x_{\mathrm{g}}^{1.4}(\mu_{\mathrm{l}} - \mu_{\mathrm{sg}})}, \qquad (44)$$

where

$$\ln\mu_{\mathrm{l}} = \left(\frac{1-y}{1-x_{\mathrm{g}}}\right)\ln\mu_{\mathrm{ml}} + \left(\frac{y-x_{\mathrm{g}}}{1-x_{\mathrm{g}}}\right)\ln\mu_{\mathrm{sl}}. \qquad (45)$$

4 Solution procedure

The accuracy of the capillary tube model can be assessed and compared using the mass flow rate as the comparison parameter instead of other parameters, owing to the drastic pressure change near the capillary tube exit[43]. Therefore, in this study, mass flow algorithms were implemented in both the homogenous flow model and separated flow model. The experimental data obtained by Melo et al.[32] include the condenser pressure (P_{cond}), evaporator pressure (P_{eva}), degree of subcooling (ΔT_{sc}), and mass flow rate (m). Schenk and Oellrich[18] measured the inlet pressure (P_{in}), inlet temperature (T_{in}), outlet temperature (T_{out}), degree of subcooling (ΔT_{sc}), mass flow rate (m), and saturated pressure corresponding to the outlet temperature ($P_{\mathrm{sat,out}}$). Therefore, various differences exist between the algorithms used to obtain these two sets of data. Additionally, the data obtained by Melo et al.[32] are based on high condensation pressures, and the mass flow rates are over 2 kg·h⁻¹. In contrast, the data obtained by Schenk and Oellrich[18] are based on lower mass flow rates, and there is no tube wall roughness parameter in their data. Additionally, we used the median of the data obtained by Melo's team and the properties of R600a were calculated using REFPROP 9.1[44].

4.1 Mass flow rate algorithm in case without metastable flow

The friction factor depends on the mass flow rate; therefore, the algorithm requires an initial estimate of the mass flow rate. The length of the capillary tube was calculated using the prescribed pressure drop (ΔP). In the case without metastable flow, the total length of the capillary tube (L_{total}) is the sum of the length of the subcooled liquid region (L_{sc}) and length of the equilibrium two-phase region (L_{egl}). The calculated total length was compared to the real capillary tube length, and the initial mass flow rate was continuously adjusted until the two lengths were equal. Fig. 3 shows the flowchart diagrams of the mass flow rate algorithm in the case without metastable flow.

4.2 Mass flow rate algorithm in case with metastable flow

In the case with metastable flow, the total length of the capillary tube (L_{total}) consists of the lengths of all four regions. Thus, the calculation of the middle two lengths was added to the mass flow rate algorithm, as shown in Fig. 4.

5 Results and discussion

5.1 Comparison of empirical correlations

Fig. 5 shows the comparison of the viscosity distributions
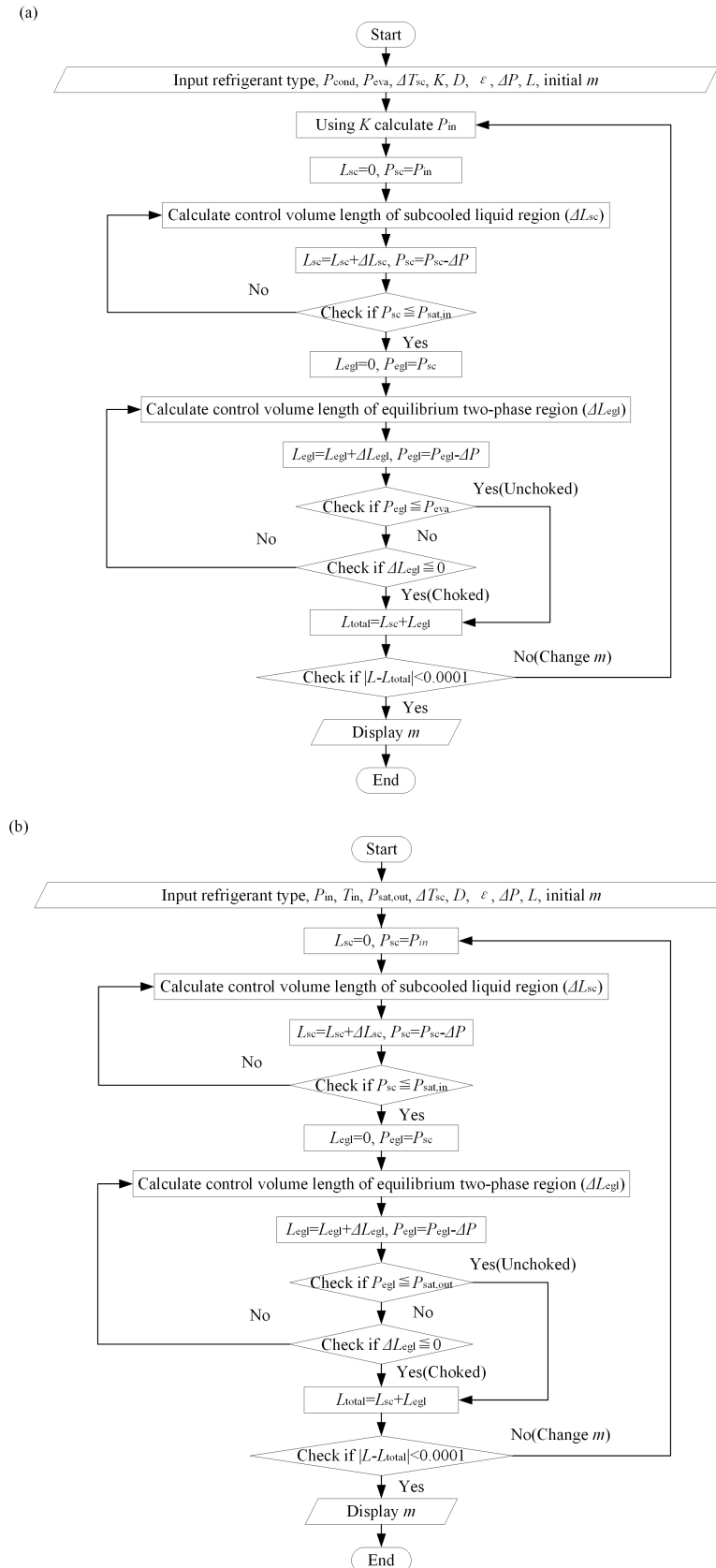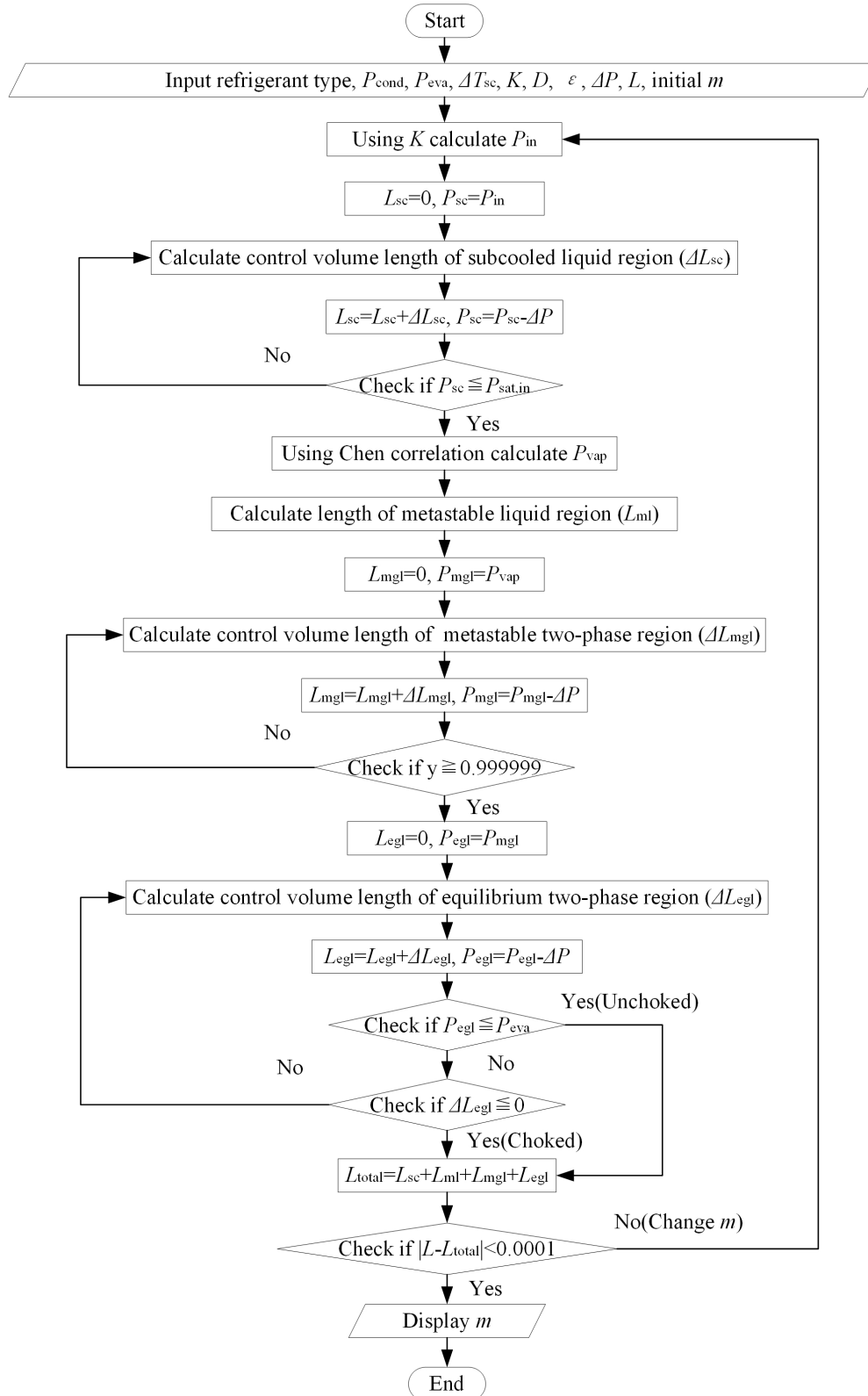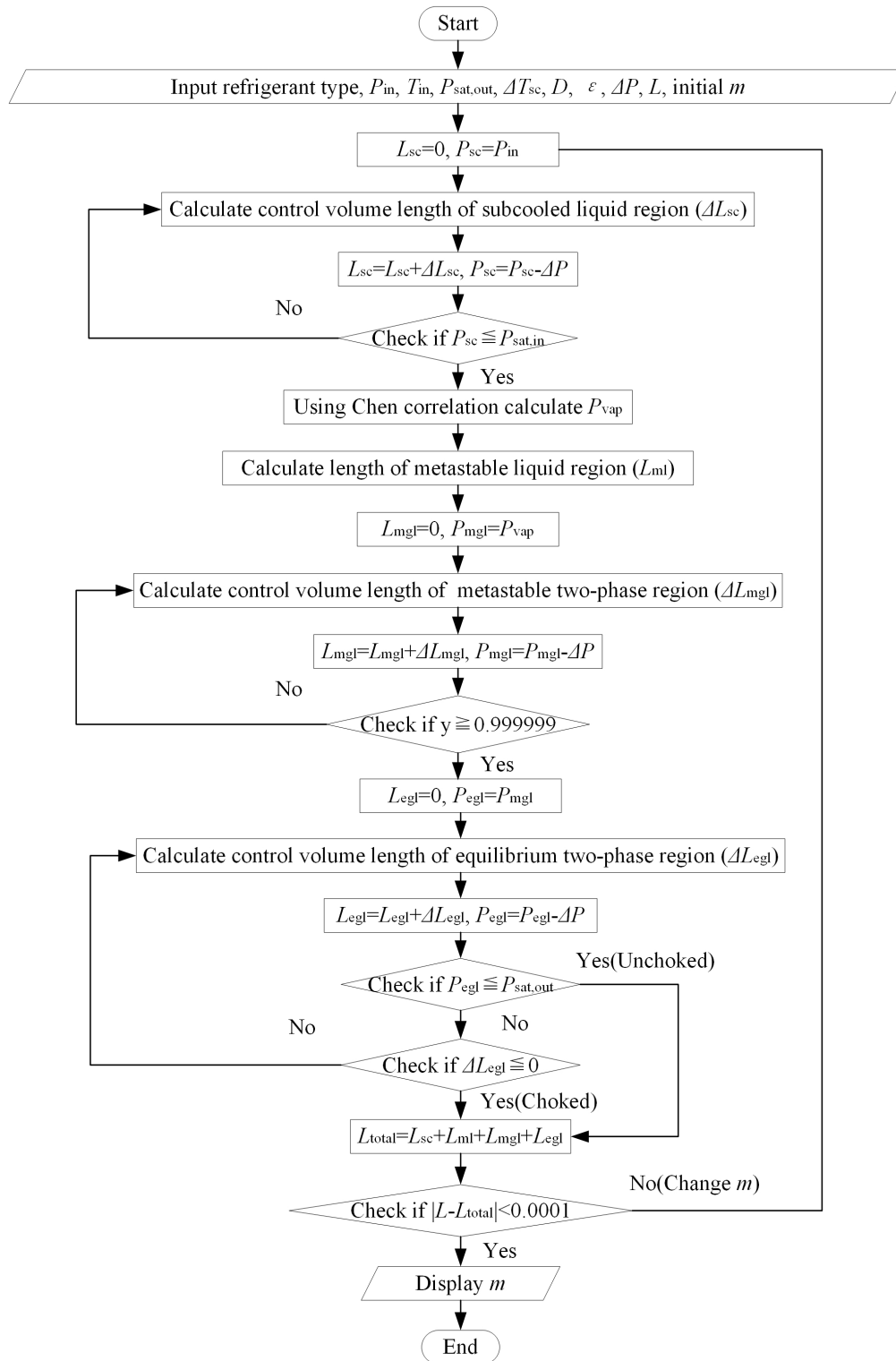
(a)

(b)

Fig. 3. Flowcharts of mass flow rate algorithm in case without metastable flow. (a) Algorithm for data of Melo et al.[32]. (b) Algorithm for data of Schenk and Oellrich[18].

along the two-phase region calculated by the three viscosity correlations and the Colebrook friction factor correlation of the two models. A typical operating condition with metastable flow was considered for comparison.

From the inlet of the two-phase region, the viscosity values calculated by all three correlations decreased along the tube owing to the increase in the volume fraction of the vapor phase. Moreover, the Lin correlation provided the largest

(a)

(b)

Fig. 4. Flowcharts of mass flow rate algorithm in case with metastable flow. (a) Algorithm for data of Melo et al.[32]. (b) Algorithm for data of Schenk and Oellrich[18].

viscosity value in the two-phase region, while the viscosity value calculated by the Dukler correlation was the smallest. The maximum discrepancy between the viscosity values calculated by the two correlations was approximately 54% at the point where the tube length was approximately 2.25 m.

Hence, the smallest mass flow rate was calculated using the Lin correlation, and the largest mass flow rate was calculated using the Dukler correlation.

Additionally, the viscosity calculated by the McAdams and Dukler correlations in the metastable two-phase region
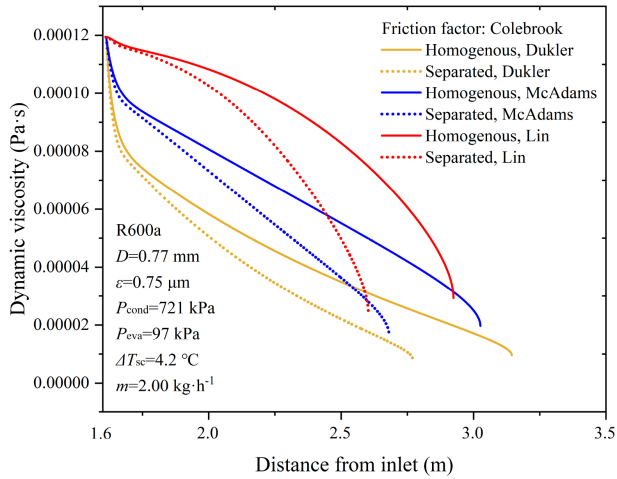
Fig. 5. Comparison of different viscosity correlations.

changes more rapidly compared with that calculated by the Lin correlations. Therefore, metastable flow is more influential when using the McAdams and Dukler correlations to calculate the two-phase viscosity.

Fig. 6 shows the friction factor distributions along the capillary tube calculated using the Dukler viscosity correlation and different friction factor correlations with metastable flow in both the homogenous flow model and separated flow model.

In the subcooled liquid region and metastable liquid region, there is no considerable difference between the friction factors calculated by the three correlations. Moreover, the values remained approximately constant throughout the entire liquid region. When the flow reached the two-phase region, the friction factors calculated by the three correlations suddenly decreased until the outlet of the capillary tube, owing to vapor phase generation.

Although the friction factors calculated by all three correlations sharply decreased, the difference between them was not obvious in the metastable two-phase region. The equilibrium two-phase region is the only region wherein the values of the friction factor calculated by the three correlations differed significantly. The largest value of the friction factor was calculated using the Colebrook correlation, whereas the Churchill
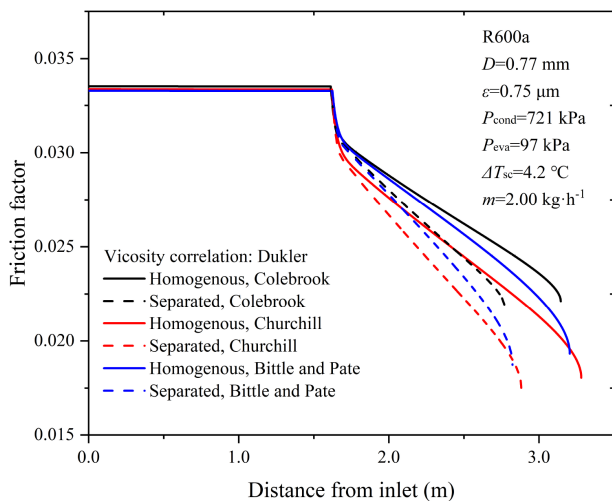
correlation provided the smallest value in the equilibrium two-phase region. The friction factor discrepancy between the values obtained by the two correlations reached a maximum of approximately 18% at the tube exit. This resulted in the smallest mass flow rate being calculated by the Colebrook correlation and the largest mass flow rate being calculated by the Churchill correlation when predicting the mass flow rate of the capillary tube.

By model comparison, it was found that the separated flow model provided a larger viscosity gradient in the two-phase region compared with the homogenous flow model, which resulted in a tendency for larger friction factor variation, as shown in Figs. 5 and 6. The tube length designed by the separated flow model was shorter by approximately 10%; therefore, the predicted mass flow rate was lower when the tube length was fixed.

5.2 Comparison of accuracy of homogenous flow model and separated flow model

Fig. 7 compares the predicted mass flow rates of the homogenous flow model and separated flow model using the Colebrook friction factor and Dukler viscosity correlations to
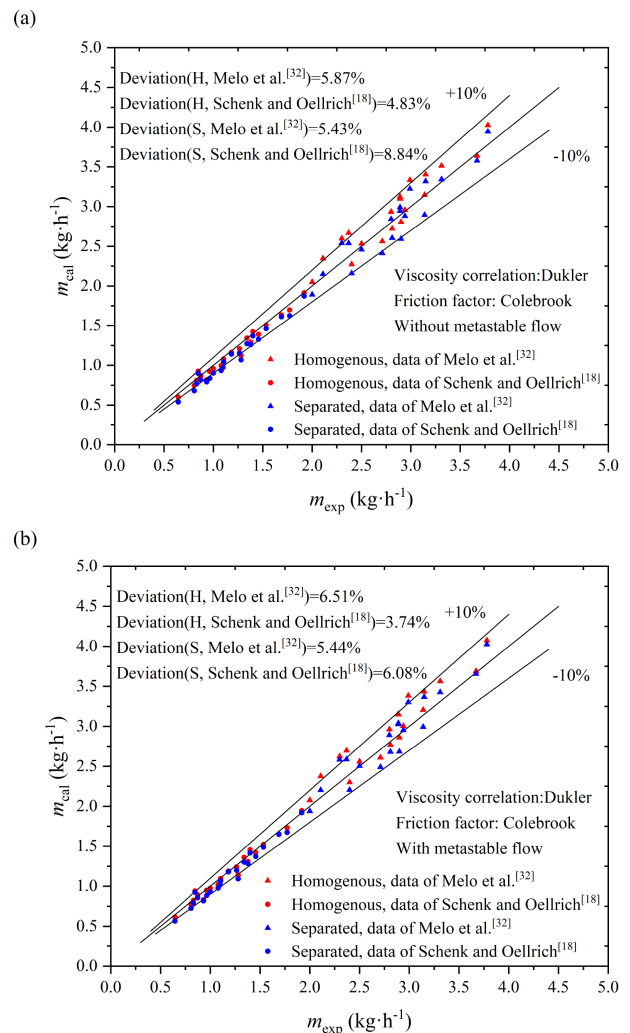
(a)

(b)

Fig. 7. Comparison of mass flow rates predicted by homogenous flow model and separated flow model to experimental data. (a) Case without metastable flow. (b) Case with metastable flow.

Fig. 6. Comparison of different friction factor correlations.

the experimental data. The cases with and without metastable flow are considered. Obviously, the mass flow rates calculated by the separated flow model are slightly lower than those predicted by the homogenous flow model. Most of the data points lie within the ±10% error band, which indicates that both models have good mass flow rate prediction accuracy. By comparing Fig. 7a and 7b, it can be found that the mass flow rates calculated with metastable flow are larger than those calculated without metastable flow, owing to the lower value of the friction factor in the equilibrium two-phase region, which resulted from the sharp decrease in the friction factor in the metastable region.

The model results calculated with different combinations of empirical correlations were compared to two sets of previously reported experimental data. Thus, the accuracy of the two proposed models with and without metastable flow was verified, and the effects of the friction factor and viscosity correlations were evaluated. The average relative deviations between the two experimental datasets and the homogenous flow model and separated flow model with different combinations of friction factor and viscosity correlations, and the impact of metastable flow are presented in Table 1.

The results reveal that, when predicting mass flow rates over 2 kg·h⁻¹, the separated flow model generally performed better than the homogenous flow model, whereas the homogenous flow model had much higher accuracy with lower mass flow rates. These results can be explained by the flow visualization work of Lorbek et al.[31]. The average velocity of the vapor phase, and the difference between the velocity of the vapor and liquid phases, increased with the mass flow rate. Therefore, the homogenous flow assumption may widely deviate from reality as the mass flow rate increases. In contrast, the flow pattern has a greater possibility of homogeneity when the mass flow rate is lower, because the flow is more susceptible to the influence of imperfections on the inner tube surface.

The separated flow model with the Colebrook friction factor correlation achieved the best prediction result relative to the data of Melo et al.[32] when metastable flow was considered. The deviations were 5.43% and 5.49%, respectively, when the Dukler and McAdams viscosity correlations were combined and metastable flow was ignored. In the case of

metastable flow, the deviations were 5.44% and 5.43%. The homogenous flow model with the Bittle and Pate friction factor and Dukler viscosity correlations achieved the most accurate prediction of the mass flow rate measured by Schenk and Oellrich[18]. The mean error was 4.12% and 3.37% when ignoring and considering the metastable flow, respectively.

5.3 Comparison of flow characteristics of homogenous flow model and separated flow model

Fig. 8 shows the pressure distributions along the capillary tube calculated by the homogenous flow model and separated flow model with and without metastable flow. The working condition and employed combination of the friction factor and two-phase viscosity correlations are the same as those in Fig. 5. The pressure dropped linearly in the liquid region until the inlet of the two-phase region, and then dropped rapidly and nonlinearly. The separated flow model exhibited faster pressure drop from the beginning of vaporization, owing to the higher vapor mass fraction, which resulted in a shorter calculated tube length and lower pressure at the tube exit. The refrigerant reached the choked flow condition at approximately 149 kPa for the homogenous flow model and 98 kPa for the separated flow model. In both models, the vaporization was delayed when metastable flow was considered. The total length of the metastable liquid region and metastable two-phase region occupied approximately 23% and 27% of the total tube length for the separated flow model and homogenous flow model, respectively. For the separated flow model, the predicted tube length increased by approximately 5.0% with metastable flow. For the homogenous flow model, the predicted tube length increased by 2.5% with metastable flow.

Fig. 9 shows the temperature distributions along the tube for the two models, with and without metastable flow. The temperature remained constant in the subcooled-liquid region and began to decrease at the beginning of vaporization. The separated flow model exhibited faster temperature drop in the two-phase region and lower temperature at the tube exit, owing to the sharper pressure drop and lower outlet pressure. The outlet temperature provided by the homogenous and separated flow models was approximately −1.5 ℃ and −12.6 ℃, respectively. The metastable flow extended the constant temperature zone, and the temperature decreased in extremely

Table 1. Comparison of accuracy of homogenous flow model and separated flow model with different friction factor and viscosity correlations.

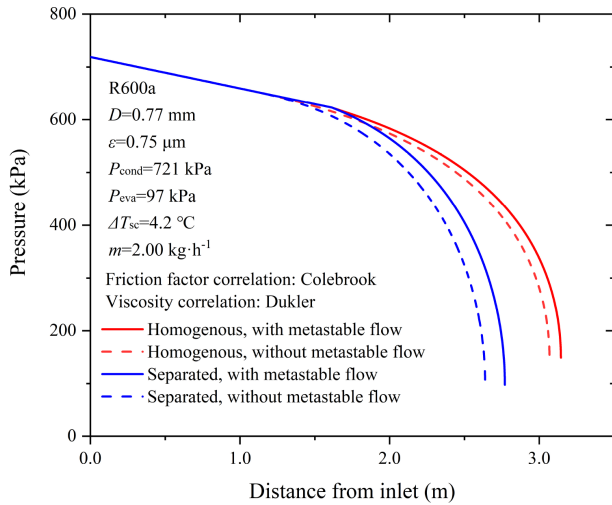| Friction factor correlation	Two-phase viscosity correlation	Average relative deviation against data of Melo et al.[32] (%)				Average relative deviation against data of Schenk and Oellrich[18] (%)			
		Without the metastable flow		With the metastable flow		Without the metastable flow		With the metastable flow	
		Homogenous flow model	Separated flow model	Homogenous flow model	Separated flow model	Homogenous flow model	Separated flow model	Homogenous flow model	Separated flow model
Colebrook	Dukler	5.87	5.43	6.51	5.44	4.83	8.84	3.74	6.08
	McAdams	5.50	5.49	5.97	5.43	6.48	10.55	4.65	7.50
	Lin	5.48	5.87	5.56	5.45	7.79	11.59	5.76	8.51
Churchill	Dukler	7.80	5.98	8.82	6.61	4.51	8.35	3.52	5.75
	McAdams	6.74	5.97	7.55	6.30	6.55	10.35	4.80	7.39
	Lin	5.96	6.02	6.69	6.00	7.96	11.43	5.95	8.53
Bittle and Pate	Dukler	6.47	5.55	7.20	5.77	4.12	7.77	3.37	5.22
	McAdams	5.72	5.59	6.38	5.55	5.58	9.44	3.89	6.38
	Lin	5.55	5.78	5.74	5.53	6.66	10.40	4.75	7.25

Fig. 8. Comparison of pressure distributions along tube.
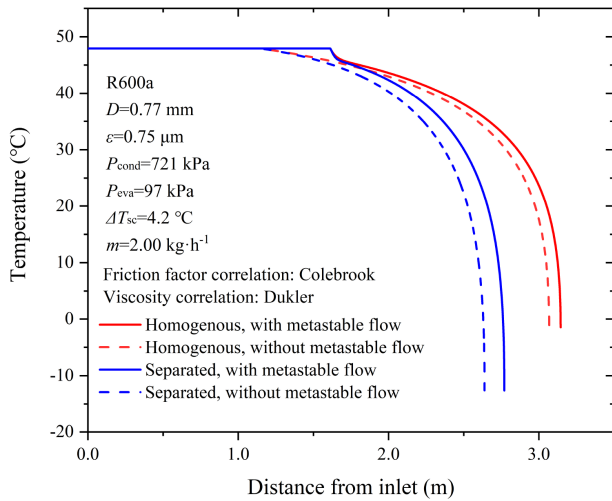

Fig. 9. Comparison of temperature distributions along tube.

rapid manner in the metastable two-phase region, owing to the existence of metastable liquid. However, the outlet temperature was hardly affected by metastable flow.

Fig. 10 shows the variation in the vapor-phase mass fraction along the two-phase region obtained by the two models. The vapor phase mass fraction gradually increased from the starting point of vaporization when metastable flow was ignored in both models. The vapor-phase mass fraction increased faster when the separated flow model was used, owing to the larger pressure gradient. At the tube outlet, the vapor-phase mass fraction obviously increased owing to the sharp pressure drop before the flow reached the choked condition. The mass fraction values of the vapor phase at the outlet were 36.6% and 32.5%, as calculated using the separated flow model and homogenous flow model, respectively. This discrepancy was caused by the lower outlet pressure provided by the separated flow model. When metastable flow was considered, the vapor phase mass fraction sharply increased in the metastable two-phase region, owing to the existence of a superheated liquid. This indicates that vapor was rapidly generated in this region, which resulted in a 2.7% and 3.6% vapor phase mass fraction at the inlet of the equilibrium two-
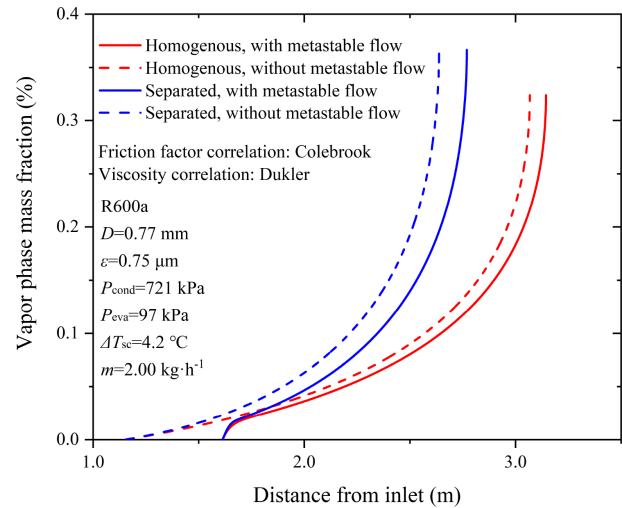

Fig. 10. Comparison of vapor phase mass fraction distributions along two-phase region.

phase region for the separated flow model and homogenous flow model, respectively.

The flow velocity discrepancy is the fundamental difference between the homogenous flow model and separated flow model. Fig. 11 illustrates the velocity distribution along the two-phase region with different models. The average refrigerant velocity for the homogenous flow model and the liquid velocity and vapor velocity for the separated flow model are shown for comparison. Regardless of which model was adopted, all calculated velocity values first increased gradually and then increased sharply near the exit as vapor was constantly generated. The velocity difference between the liquid and vapor phases increased from the inlet to the outlet when the separated flow model was used. For the homogenous model, the average velocity of the refrigerant is between the liquid and vapor phase values of the separated flow model. At the capillary tube exit, the average velocity calculated by the homogenous flow model, and the liquid velocity and vapor velocity calculated by the separated flow model, are approximately 97 m·s⁻¹, 19 m·s⁻¹, and 171 m·s⁻¹, respectively. For both the homogenous flow model and separated flow model, the
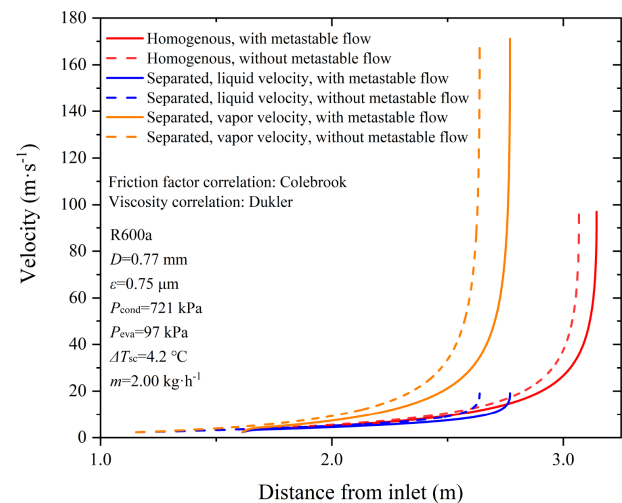

Fig. 11. Comparison of velocity distributions along two-phase region.

metastable flow had negligible impact on the flow velocity.

6   Conclusions

This study presents a comprehensive comparative investigation of the homogenous flow model and separated flow model, which were used to simulate R600a flowing through adiabatic capillary tubes. The models were established with and without metastable flow to investigate the influence of the metastable phenomenon. Various friction factors and two-phase viscosity correlations were tested to determine the optimal combination of empirical correlations. Two sets of previously reported experimental data with different mass flow rate ranges were used as references to validate the models. Through the analysis and comparison of the numerical results, the following conclusions were drawn:

（Ⅰ）The separated flow model performs better when predicting mass flow rates over 2 kg·h^{-1}, whereas the homogenous flow model has higher accuracy at a lower mass flow rate range, possibly owing to flow pattern discrepancy with different mass flow rate ranges.

（Ⅱ）Compared with the mass flow rate data over 2 kg·h^{-1}, the separated flow model with the Colebrook friction factor correlation combined with the Dukler or McAdams viscosity correlation achieved better prediction. The deviations were 5.43%, 5.49% and 5.44%, 5.43% when ignoring and considering metastable flow, respectively.

（Ⅲ）The homogenous flow model with the Bittle and Pate friction factor and Dukler viscosity correlations achieved the most accurate prediction of mass flow rate data under 2 kg·h^{-1}. The mean errors were 4.12% and 3.37% when ignoring and considering metastable flow, respectively.

（Ⅳ）The separated flow model provided more drastic pressure drop and temperature drop, owing to the larger vapor-phase mass fraction and higher vapor velocity compared with the homogenous flow model, which resulted in the prediction of a lower mass flow rate by the separated flow model.

Acknowledgements

Conflict of interest

The authors declare that they have no conflict of interest.

Biographies

Yonghui Shu   is currently a Master's student under the tutelage of Prof. Peng Hu at the University of Science and Technology of China. His research interests include refrigeration and cryogenics.

Peng Hu   received his Ph.D. degree in Engineering Thermophysics from the University of Science and Technology of China (USTC). He is currently a professor at USTC. His research interests include thermophysical properties, refrigeration, heat and mass transfer, and solar energy.

References

[1] Ali M S, Anwar Z, Mujtaba M A, et al. Two-phase frictional pressure drop with pure refrigerants in vertical mini/micro-channels. *Case Studies in Thermal Engineering,* **2021**, *23*: 100824.

[2] Zhang N C, Li B, Feng L H, et al. Research on the thermophysical properties and cycle performances of R1234yf/R290 and R1234yf/R600a. *International Journal of Thermophysics,* **2021**, *42*: 123.

[3] Zhang N, Hu P, Chen L X, et al. Measurements of critical properties of the binary mixture of 1,1,1-trifluoroethane (HFC-143a)+ *trans*-1,3,3,3-Tetrafluoropropene (HFO-1234ze (E)). *Journal of Chemical & Engineering Data,* **2021**, *66*: 2717–2722.

[4] Bagherzadeh S A, D'Orazio A, Karimipour A, et al. A novel sensitivity analysis model of EANN for F-MWCNTs-Fe$_3$O$_4$/EG nanofluid thermal conductivity: Outputs predicted analytically instead of numerically to more accuracy and less costs. *Physica A: Statistical Mechanics and its Applications,* **2019**, *521*: 406–415.

[5] Giwa S O, Sharifpur M, Goodarzi M, et al. Influence of base fluid, temperature, and concentration on the thermophysical properties of hybrid nanofluids of alumina–ferrofluid: Experimental data, modeling through enhanced ANN, ANFIS, and curve fitting. *Journal of Thermal Analysis and Calorimetry,* **2021**, *143*: 4149–4167.

[6] Sánchez D, Cabello R, Llopis R, et al. Energy performance evaluation of R1234yf, R1234ze(E), R600a, R290 and R152a as low-GWP R134a alternatives. *International Journal of Refrigeration,* **2017**, *74*: 269–282.

[7] Hwang S, Jeong J H. The effects of the parameters of a refrigeration system working with R600a on the non-equilibrium subcooled two-phase flow of the refrigerant. *International Journal of Refrigeration,* **2020**, *118*: 462–469.

[8] Bahmani M H, Sheikhzadeh G, Zarringhalam M, et al. Investigation of turbulent heat transfer and nanofluid flow in a double pipe heat exchanger. *Advanced Powder Technology,* **2018**, *29* (2): 273–282.

[9] Sarafraz M M, Tian Z, Tlili I, et al. Thermal evaluation of a heat pipe working with *n*-pentane-acetone and *n*-pentane-methanol binary mixtures. *Journal of Thermal Analysis and Calorimetry,* **2020**, *139*: 2435–2445.

[10] Heimel M, Lang W, Berger E, et al. A homogeneous capillary tube model - comprehensive parameter studies using isobutane as refrigerant. In: International Refrigeration and Air Conditioning Conference. West Lafayette: Purdue University, 2012: Paper 1233.

[11] de Lara J F, Melo C, Boeng J, et al. Experimental analysis of HFC-134a expansion through small-bore adiabatic capillary tubes. *International Journal of Refrigeration,* **2020**, *112*: 37–43.

[12] Ardhapurkar P M, Sridharan A, Atrey M D. Investigation of pressure drop in capillary tube for mixed refrigerant Joule-Thomson cryocooler. *AIP Conference Proceedings,* **2014**, *1573*: 155.

[13] Kruthiventi S S H, Venkatarathnam G. Studies on capillary tube expansion device used in J-T refrigerators operating with nitrogen-hydrocarbon mixtures. *Cryogenics,* **2017**, *87*: 76–84.

[14] Parmar D, Atrey M D. Experimental and numerical investigation on the flow of mixed refrigerants through capillary tubes at cryogenic temperatures. *Applied Thermal Engineering,* **2020**, *175*: 115339.

[15] Rocha T T M, de Paula C H, Cangussu V M, et al. Effect of surface roughness on the mass flow rate predictions for adiabatic capillary tubes. *International Journal of Refrigeration,* **2020**, *118*: 269–278.

[16] Khan M K, Kumar R, Sahoo P K. Flow characteristics of refrigerants flowing through capillary tubes-A review. *Applied Thermal Engineering,* **2009**, *29*: 1426–1439.

[17] García-Valladares O. Numerical simulation and experimental validation of coiled adiabatic capillary tubes. *Applied Thermal Engineering,* **2007**, *27*: 1062–1071.

[18] Schenk M, Oellrich L R. Experimental investigation of the refrigerant flow of isobutane (R600a) through adiabatic capillary tubes. *International Journal of Refrigeration,* **2014**, *38*: 275–280.

[19] Chingulpitak S, Wongwises S. Two-phase flow model of refrigerants flowing through helically coiled capillary tubes. *Applied Thermal Engineering,* **2010**, *30*: 1927–1936.

[20] Vinš V, Hrubý J, Vacek V. Numerical simulation of gas-contaminated refrigerant two-phase flow through adiabatic capillary tubes. *International Journal of Heat and Mass Transfer,* **2010**, *53*: 5430–5439.

[21] Rasti M, Jeong J H. A generalized continuous empirical correlation for the refrigerant mass flow rate through adiabatic straight and helically coiled capillary tubes. *Applied Thermal Engineering,* **2018**, *143*: 450–460.

[22] Hermes C J L, Melo C, Knabben F T. Algebraic solution of capillary tube flows Part I: Adiabatic capillary tubes. *Applied Thermal Engineering,* **2010**, *30*: 449–457.

[23] Dubba S K, Kumar R. Flow of refrigerants through capillary tubes: A state-of-the-art. *Experimental Thermal and Fluid Science,* **2017**, *81*: 370–381.

[24] Jadhav P, Agrawal N. A comparative study in the straight and a spiral adiabatic capillary tube. *International Journal of Ambient Energy,* **2019**, *40*: 693–698.

[25] Alok P, Sahu D. Numerical simulation of capillary tube for selected refrigerants using homogeneous equilibrium model. *International Journal of Air-Conditioning and Refrigeration,* **2019**, *27*: 1950001.

[26] Jadhav P, Agrawal N. A comparative study of flow characteristics of adiabatic spiral and helical capillary tube in a CO_2 transcritical system. *International Journal of Ambient Energy,* **2021**: 1–8.

[27] Zareh M, Heidari M G, Javidmand P. Numerical simulation and experimental comparison of the R12, R22 and R134a flow inside straight and coiled helical capillary tubes. *Journal of Mechanical Science and Technology,* **2016**, *30*: 1421–1430.

[28] Wang J, Cao F, Wang Z Z, et al. Numerical simulation of coiled adiabatic capillary tubes in CO_2 transcritical systems with separated flow model including metastable flow. *International Journal of Refrigeration,* **2012**, *35* (8): 2188–2198.

[29] Agrawal N, Bhattacharyya S. Homogeneous versus separated two phase flow models: Adiabatic capillary tube flow in a transcritical CO_2 heat pump. *International Journal of Thermal Sciences,* **2008**, *47* (11): 1555–1562.

[30] Furlong T W, Schmidt D P. A comparison of homogenous and separated flow assumptions for adiabatic capillary flow. *Applied Thermal Engineering,* **2012**, *48*: 186–193.

[31] Lorbek L, Kuhelj A, Dular M, et al. Two-phase flow patterns in adiabatic refrigerant flow through capillary tubes. *International Journal of Refrigeration,* **2020**, *115*: 107–116.

[32] Melo C, Ferreira R T S, Neto C B, et al. An experimental analysis of adiabatic capillary tubes. *Applied Thermal Engineering,* **1999**, *19*: 669–684.

[33] Collier J G, Thome J R. Convective Boiling and Condensation. 3rd ed. New York: Clarendon Press, 1994.

[34] Chen Z H, Li R Y, Lin S, et al. A correlation for metastable flow of R-12 through capillary tubes. *ASHRAE Transactions,* **1990**, *96*: 550–554.

[35] Feburie V, Giot M, Granger S, et al. A model for choked flow through cracks with inlet subcooling. *International Journal of Multiphase Flow,* **1993**, *19*: 541–562.

[36] Premoli A, Francesco D, Prina A. An empirical correlation for evaluating two-phase mixture density under adiabatic conditions. In: European Two-Phase Flow Group Meeting, Milan, Italy, 1970.

[37] Chisholm D. Pressure gradients due to friction during the flow of evaporating two-phase mixtures in smooth tubes and channels. *International Journal of Heat and Mass Transfer,* **1973**, *16*: 347–358.

[38] Deodhar S D, Kothadia H B, Iyer K N, et al. Experimental and numerical studies of choked flow through adiabatic and diabatic capillary tubes. *Applied Thermal Engineering,* **2015**, *90*: 879–894.

[39] Chung M. A numerical procedure for simulation of Fanno flows of refrigerants or refrigerant mixtures in capillary tubes. 1998 ASHRAE Summer Annual Meeting, 1998 [2021-04-10]. https://www.osti.gov/biblio/687663-numerical-procedure-simulation-fanno-flows-refrigerants-refrigerant-mixtures-capillary-tubes.

[40] Zhang Y F, Zhou G B, Xie H, et al. An assessment of friction factor and viscosity correlations for model prediction of refrigerant flow in capillary tubes. *International Journal of Energy Research,* **2005**, *29* (3): 233–248.

[41] Ahmadi M H, Mohseni-Gharyehsafa B, Ghazvini M, et al. Comparing various machine learning approaches in modeling the dynamic viscosity of CuO/water nanofluid. *Journal of Thermal Analysis and Calorimetry,* **2020**, *139*: 2585–2599.

[42] Zhou G B, Zhang Y F. Numerical and experimental investigations on the performance of coiled adiabatic capillary tubes. *Applied Thermal Engineering,* **2006**, *26*: 1106–1114.

[43] Bansal P K, Wang G. Numerical analysis of choked refrigerant flow in adiabatic capillary tubes. *Applied Thermal Engineering,* **2004**, *24*: 851–863.

[44] Lemmon E, Huber M, McLinden M. NIST Standard Reference Database 23: NIST thermodynamic and transport properties of refrigerants and refrigerant mixtures-REFPROP, version 9.1. Gaithersburg, MD: National Institute of Standards and Technology, 2013.